

# MONITORING TREE MOISTURE USING AN INVERSION ALGORITHM APPLIED TO SAR DATA FROM BOREAS

Mahta Moghaddam and Sasan Saatchi  
Jet Propulsion Laboratory, MS 300-235  
California Institute of Technology  
4800 Oak Grove Drive  
Pasadena, CA 91109

## ABSTRACT

During several field campaigns in spring and summer of '94, the NASA/JPL airborne synthetic aperture radar (AIRSAR) collected data over the southern and northern study sites of BOREAS. Among the areas over which radar data were collected was the young jack pine (YJP) tower site, which is generally characterized as having short (2-4 m) but closely spaced trees with a dense crown layer. In this work, the AIRSAR data over this YJP stand from six different dates are used, and the dielectric constant and hence the moisture content of its branch layer components are estimated. This is accomplished by first deriving a parametric scattering model from a numerical discrete-component forest model. This is possible if the predominant scattering mechanism can be identified. Here, a classification algorithm is used for this purpose, concentrating on areas where the volume scattering mechanism from the branch layer dominates. Once the parametric model is derived, a nonlinear estimation algorithm is employed to retrieve the model parameters from SAR data. This algorithm is iterative, and takes the statistical properties of the data and unknown parameters into account. This inversion process is first verified using synthetic data, after which it is applied to AIRSAR data of 130 REAS. The results show how the environmental conditions affected the moisture state of this forest stand over a period of six months. They are also compared in detail to the available ground-truth measurements from the area.

## 1. INTRODUCTION

Boreal forests cover a large area of the Northern hemisphere and have been the subject of many investigations in order to characterize their role in global biogeochemical cycles and climate studies. The area used for this work is part of a larger region used in the boreal ecosystem atmosphere study (130 REAS) project [I]. During several focused and intensive field campaigns in 1994, the NASA/JPL airborne synthetic aperture radar (AIRSAR) acquired images over BOREAS study sites with the intention of mapping forest types and estimating parameters important in ecosystem modeling. The AIRSAR measures polarimetric C-, L-, and P-band radar backscattering data. The images chosen in this study were acquired over an area containing primarily jack pine stands: young jack pine (YJP) at a regeneration stage with average age of 10-15 years, and old jack pine (OJP) with average age of 65 years. These are located in the BOREAS Southern study area (SSA), near the Prince Albert National Park in Saskatchewan.

In this work, data from six different days in 1994 were used: 17, 20, and 26 April, 11 June, 28 July, and 20 September. The three April data sets span the thaw season. The remaining three data sets represent the state of the forest during the spring and summer growing seasons.

The young jack pine (YJP) stand was well characterized by performing comprehensive ground truth measurements. The quantities measured are related to the structure and architecture of the forest canopy, which are slowly varying functions of time, and on small time scales (days, weeks, or even months), not dependent on environmental conditions such as temperature and precipitation. To study the interaction of the forest stand with the atmosphere, energy exchanges, and growth rate, it is necessary to measure parameters which are more dynamically related to changes in the environmental conditions. One such parameter is the moisture content of the canopy, which is directly related to the dielectric constant of the forest canopy components, and hence can, in principle, be obtained with scattering measurements using SAR. The SAR can provide such data on arbitrarily small time scales from an airborne platform, and periodic coverage of the order of a few

clays if operated from a spaceborne platform. It can also acquire data regardless of cloud and smoke coverage or sun illumination. It is hence the instrument of choice for quantitative retrieval of canopy moisture content if appropriate algorithms are applied.

In this work, our goal is to determine the moisture content of the branch layer components in the YJP forest by estimating dielectric constant values from SAR data. Polarimetric AIRSAR data will be used here, but the methodology can also be used with spaceborne SAR data if polarimetric measurements are available. Several researchers in recent years have addressed the problem of relating radar observations to the bio- and geophysical parameters of forests, a few examples of which are given in [2-11]. Their works can be grouped into two categories: one in which the interpretation is of a qualitative nature, as in classification algorithms, and the other where an attempt is made to quantitatively estimate the parameters describing the forests. Among the former category are those of [2,3], with a comprehensive account given in [4]. The latter group of works have concentrated on retrieval of target parameters from radar scattering data using empirical and/or theoretical methods. For example, biomass retrieval has been addressed in many studies [5-7] using mainly experimental data to obtain empirical regression models. These are highly useful, but are only accurate in specific areas for which the empirical relations have been derived. Scattering models have been incorporated in another group of methods to construct and train neural networks to estimate forest scattering parameters [9-11]. These methods are more flexible and universal, but since they involve many unknown parameters, training times are long and must be repeated for every new scene. Here, a scheme is devised which utilizes many elements of the above techniques: a classification algorithm is used to isolate appropriate scattering mechanisms and limit the number of unknowns; ground-truth information and theoretical scattering models are used to obtain parametric models relating a small number of unknowns to radar measurements; an estimation algorithm is finally employed to retrieve the unknowns. This approach yields specific quantitative estimates of forest parameters, it is fast, and it provides physical insight into the retrieval problem. A major application of this type of inversion algorithm, where one or two specific parameters can be retrieved assuming all others are known, is in monitoring temporal

change in the canopy status with respect to that parameter. In the present case, the parameters of interest are the real and imaginary parts of dielectric constant of branch-layer components, or the branch-layer moisture content. The algorithm can be summarized as follows:

1. Derive parametric models that relate the radar backscatter cross section for multiple frequencies and polarizations to the complex dielectric constant of branch layer components. In this paper, the focus is on cases where the radar backscatter is dominated by the branch layer volume scattering. The treatment of the problem for situations where mixed scattering mechanisms are important (for example trunk-ground double bounce in addition to branch layer volume scattering) is left to a future paper. The YJP forest has a rather dense crown layer, so that in fact at C- and L-bands, the backscattering cross section is almost entirely due to branch layer volume scattering (except for data from the beginning of thaw season, as explained in 4.2.1). This has been verified by using a classification algorithm [2] as well as with model calculations [12].
2. Given the parametric models, use a nonlinear optimization scheme to estimate the real and imaginary parts of the dielectric constant from SAR data [13,14]. The estimation algorithm used here is an iterative one, and includes provisions for treating the statistical properties of the data and the unknowns, as well as the ill-conditioned nature of the problem.

The above two steps will be discussed in Sections 2 and 3, respectively. The results of application of this algorithm to synthetic data will be presented in Section 4 for verification. The algorithm is then applied to BOREAS AIRSAR data, from which both the real and imaginary parts of the dielectric constant show an increasing trend from April to September, although with varying rates. These results are then compared to ground-truth measurements of dielectric constant and moisture content where available.

## 2. PARAMETRIC SCATTERING MODELS

In what follows, dielectric constant refers to the relative dielectric constant. The backscattered field from a forest contains contributions from four major sources: forest floor, double-bounce between trunks and ground, double-bounce between crown

and ground, and crown layer volume scattering. Since only a limited number of measurements are available for each pixel of SAR data, it is not possible to retrieve the parameters contributing to all the above mechanisms. Rather, cases where the scattered fields are mainly due to a single mechanism are considered. Here, we will focus on branch layer volume scattering, which can be shown (by a classification algorithm and model calculations) to be the dominant contributor in the YJP forest in the BOREAS southern study site for L- and C-bands. The P-band data were excluded from this analysis, since at that frequency, in addition to the volume scattering mechanism, the double-bounce scattering mechanisms have an important role in the total radar backscatter. For a detailed discussion of scattering mechanisms for this BOREAS site, see [12]. For the sake of brevity, further discussion of the classification algorithm [2] will not be included here.

To derive a parametric model for volume scattering from branches, a number of numerical forest scattering models could be used [15-20]. We have chosen to use the discrete component model developed at JPL by Durden et al. [15-16], which has been shown to produce backscatter values which are in very good agreement with SAR measurements. This model takes the branch layer to consist of randomly oriented finite dielectric cylinders with a  $\sin^4\alpha$  distribution, where  $\alpha$  is the angle about the mean orientation angle with respect to the vertical, the tree trunks to be randomly located nearly vertical long dielectric cylinders, and the ground to be a Bragg rough surface. The total radar backscatter is then calculated by adding volume scattering from the branch layer, double-bounce scattering between the ground and the branch and/or trunk layers, and scattering off the rough ground. Here, a forest was characterized using the ground truth measurements of YJP, and the radar backscatter was calculated for L- and C-bands for all polarizations as the real and imaginary parts of the dielectric constant of branch layer constituents were varied. These are the primary and secondary branches and needles, all assumed to have the same dielectric constant values. Although this is not entirely true for trees in general, it is a good approximation. Furthermore, since ground-truth measurements do not exist for dielectric constants of each of these components, even if slightly different dielectric values are assumed, they cannot be compared to measurements for verification. The range of variations of the real and imaginary

parts of the dielectric constant was chosen to represent the ‘{typical” observed values. It was assumed that the dielectric constants do not change significantly between L- and C-bands. This assumption was based on the works described in [21-22], where dielectric values for a conifer forest are observed not to vary significantly for L- and C-bands. As mentioned previously, here only the case where branch-layer volume scattering is the only dominant scattering mechanism is considered. Table 1 gives the ground-truth measurements of the YJP stand’s architectural parameters. These were fixed in the scattering model. The synthetic data generated from the model are shown in Figures 1(a)-1 (b) and 2(a) -2(c), respectively, for L- and C-bands. Incidence angle was set to 42 degrees, since for all the SAR data sets used here, the YJP stand was located at incidence angles between 40 and 45 degrees. As was shown in [12], the backscatter cross section due to volume scattering does not change significantly for this incidence angle range. We will exclude L-band HH’ polarization from our study, since it was found that for this channel, the results of the scattering model and the SAR data are not in sufficient agreement [12]. Furthermore, the L-HH backscatter is sensitive to the trunk-ground double-bounce mechanism, violating the assumption that volume scattering is predominant.

In each graph, the horizontal axis represents the real part of the dielectric constant, and the family of curves are generated by changing the imaginary part of the dielectric constant. Note that for a given real part, the radar backscatter decreases with increasing imaginary part. This is due to increased attenuation within the canopy. On the other hand, for a given imaginary part, the backscattered signal increases with increasing real part of the dielectric constant, since for a sparse collection of dielectric cylinders with random radius distribution, the average backscattering amplitude increases as the real part of dielectric increases. It has also been assumed that the real and imaginary parts of the dielectric are independent of each other. While this is true from a scattering point of view, and although the knowledge of one does not determine the other, in practice the knowledge of one can put constraints on the value of the other [24-25, 27,29]. Here, this type of constraint has not been imposed in the estimation problem, and the estimation is carried out for the general case of two independent unknowns.

To obtain the parametric expressions for backscattering cross section, two-dimensional polynomials were used to fit the data. This was done by performing a  $\chi^2$  fit, first to each of the curves with constant imaginary part,  $\epsilon_i$ , as a function of the real part,  $\epsilon_r$ , to get expressions of the form

$$\sigma^{B,qp}(\epsilon_r, \epsilon_i) = a_0^{B,qp}(\epsilon_i) + a_1^{B,qp}(\epsilon_i) * \epsilon_r + a_2^{B,qp}(\epsilon_i) * \epsilon_r^2 + \dots \quad (1)$$

Here,  $qp$  represents HH, VV, or HV polarizations, and  $B$  is one of L- or C-bands. These in turn were used in another series of  $\chi^2$  fits to obtain  $a_i^{B,qp}$  as

$$a_i^{B,qp}(\epsilon_i) = b_0^{B,qp} + b_1^{B,qp} * \epsilon_i + b_2^{B,qp} * \epsilon_i^2 + \dots \quad (2)$$

Here, the  $b$  coefficients are in general dependent on all the other canopy parameters, which are assumed known. It was found that polynomials of up to fourth order were required to obtain  $\chi^2$  errors of less than 0.1%. Once the  $a$  and  $b$  coefficients were found, these closed-form parametric expressions were used in an iterative inversion algorithm, which is a nonlinear estimation procedure.

There are several benefits gained from using a polynomial fit to obtain the parametric scattering expressions: Accurate fits can be obtained with only a few terms in the polynomial. The degree of accuracy can be increased readily by simply adding more (higher-order) terms if necessary. The iterative inversion process converges rapidly and is more robust than if more complicated functions were used, since the partial derivatives of the parametric expressions are smooth and well defined. The various orders of dependence of the data on the unknowns are separated and expressed as independent functions (powers of  $\epsilon$ ). By doing so, the degree of nonlinearity of the problem is explicitly described. In short, this choice provides both mathematical ease and physical insight into the estimation problem.

### 3. ESTIMATION ALGORITHM

The estimation technique (also loosely referred to as inversion technique) is a nonlinear one, since the data and unknowns are related via nonlinear functions, in this case polynomials of order up to 4. The parameter estimates are obtained by defining a least squares criterion based on minimizing the distance between data and

model calculations, which is carried out in an iterative fashion, each time updating the solution for the unknowns until an acceptably small error is reached.

Let us generically denote the nonlinear model of scattering by  $\mathbf{f}_{nl}(\mathbf{X})$ , where  $\mathbf{X}$  is the vector containing the unknown parameters and  $\mathbf{f}_{nl}$  is a nonlinear (hence the subscript *nl*) functional of  $\mathbf{X}$ . Here, the elements of  $\mathbf{X}$  are the real and imaginary parts of dielectric constant. Further, let  $\mathbf{d}_{meas}$  be the vector of SAR measured data. This vector contains the magnitude of L- and C-band multipolarized backscattering cross sections in our case. The inverse problem then can be stated as the problem of finding  $\mathbf{X}$  such that  $\mathbf{f}_{nl}(\mathbf{X})$  and  $\mathbf{d}_{meas}$  are "close." Equivalently, an  $\mathbf{X}$  must be found such that a least-squares measure  $L(\mathbf{X})$  given by

$$L(\mathbf{X}) = \frac{1}{2} \left\{ \|\mathbf{f}_{nl}(\mathbf{X}) - \mathbf{d}_{meas}\|^2 + \|\mathbf{X} - \mathbf{X}_{ap}\|^2 \right\} \quad (3)$$

is minimized. Here,  $\|\cdot\|$  denotes the  $L_2$  norm, and  $\mathbf{X}_{ap}$  is an a priori estimate of  $\mathbf{X}$ , which could be arbitrarily different from the true solution for  $\mathbf{X}$ .

Since the variability of the scattering scene can be represented as a random variable, and the SAR data are random processes, care must be taken in defining the norms in Equation (3). We take the stochastic nature of the unknown  $\mathbf{X}$  and data  $\mathbf{d}_{meas}$  into account by writing the above norms as

$$\|\mathbf{f}_{nl}(\mathbf{X}) - \mathbf{d}_{meas}\|^2 = (\mathbf{f}_{nl}(\mathbf{X}) - \mathbf{d}_{meas})^t \cdot \overline{\mathbf{C}}_d^{-1} \cdot (\mathbf{f}_{nl}(\mathbf{X}) - \mathbf{d}_{meas}), \quad (4)$$

$$\|\mathbf{X} - \mathbf{X}_{ap}\|^2 = (\mathbf{X} - \mathbf{X}_{ap})^t \cdot \overline{\mathbf{C}}_{X_{ap}}^{-1} \cdot (\mathbf{X} - \mathbf{X}_{ap}), \quad (5)$$

where  $\overline{\mathbf{C}}_d$  and  $\overline{\mathbf{C}}_{X_{ap}}$  are data and a priori estimate covariance operators, respectively. The data covariance operator represents the statistics of the data including noise. It can be thought of as a measure of "closeness" of  $\mathbf{d}_{meas}$  to  $\mathbf{f}_{nl}$ . Similarly,  $\overline{\mathbf{C}}_{X_{ap}}$  includes a priori information about the statistics of unknown parameters, and is also a measure of reliability of the a priori estimates [23]. For example, if in a given problem there is no reliable a priori estimates for the unknowns, it is advantageous to minimize the role of the second norm in Equation (3). This is automatically accomplished by observing that in such a case, the elements of the covariance operator will be large, and hence those of  $\overline{\mathbf{C}}_{X_{ap}}^{-1}$  will be very small, rendering the norm

very small compared to the first term in Equation (3). If the data components are statistically independent, the data covariance matrix will be diagonal. The same is true for the a priori covariance matrix if the parameters to be estimated in each pixel are independent. In addition to providing information about the statistics of the problem, these covariances allow the inclusion of weighting factors to improve the ill-conditioning of the inverse problem. This can be accomplished by multiplying the diagonal elements of these operators by appropriate constants, which are usually chosen such that the diagonal elements are of the same order of magnitude.

Once the above norms, or distances, are defined properly, the least-squares measure  $L(X)$  in Equation (3) can be minimized by carrying out the following steps in an iterative fashion:

1. Obtain an initial estimate for  $X$ . This is  $X_{ap}$ , and can be found either from previous measurements of  $X$ , or by simply assigning an arbitrary value to it.
2. Calculate an estimate to the data by using the latest estimate of  $X$ , i.e., find  $f_{nl}(X)$ .
3. Find  $I(X)$ . This assumes the knowledge of the covariance operators. If  $L$  is small enough, the solution has been found; terminate the iterations. Continue otherwise.
4. Find the direction of update for  $X$ .
5. Find the step length in the direction of update.
6. Update the solution to  $X$  by moving in the direction found in 4 by the length found in 5.
7. Go to step 2.

Several methods can be used in steps 4 and 5 to find the update direction and step size for the unknown. We have used a preconditioned conjugate gradient method, which has an improved convergence behavior over the conventional conjugate gradient solution. This algorithm is outlined in the Appendix.

## 4. RESULTS

### 4.1. Verification

This algorithm was first tested as follows: Synthetic data were generated using the above-mentioned numerical forest scattering model with the parameters of Table 1. The simulations were carried out for several different values of complex dielectric constant. First, it was assumed that the imaginary part of the dielectric constant is known and the value of the real part was estimated (Figure 3(a)). Next, the real part was assumed known and the imaginary part was estimated (Figure 3(b)). Finally, both parameters were taken to be unknowns (Figure 3(c)). From these Figures it is observed that the estimation error for “typical” values of the dielectric constant is generally less than 10%, and for all other cases is less than 25%. Note that given the numerous uncertainties and errors in data measurement and calibration, as well as in ground-truth measurements, a retrieval error bounded by 25% is acceptable. It is also observed that the estimation error is larger for smaller values of imaginary part of dielectric, since in this case the parametric models are more nonlinear than when they are larger, and hence the estimation algorithm becomes less accurate as expected. Furthermore, the errors are smaller when only one of the parameters is unknown; for the same values of the real and imaginary parts of the dielectric constant, the error in inversion is larger if neither of them is assumed known. In summary, the above tests verify the accuracy of the parametric models and the inversion algorithm, indicating that with perfect data and for typical parameter ranges, the estimation errors committed will be no more than about 10%.

### 4.2. BOREAS AIRSAR Data

We now turn to BOREAS AIRSAR data taken over the young jack pine (YJP) stand in the Southern study area (SSA) during the 1994 field campaigns. A sample radar image is shown in Figure 4. This is an R-G-B overlay of P-band, L-band, and C-band of total power radar backscattering cross section, obtained on July 11, 1994. Figures 5 and 6 show, respectively, the variation in C- and L-band radar backscatter over the chosen six data takes for this area. No P-band data were used

throughout this work, since at P-band, the backscattering from the YJP stand is no longer dominated by branch layer volume scattering, but includes significant effects from the trunk-ground and branch-ground double-bounce mechanisms [12]. The error bars in the figures show the standard deviation of the backscatter within the canopy calculated using 30 different locations, each consisting of 25 pixels (5 x 5) of 16-look SAR data. We observe that at each frequency, all polarizations show similar trends with respect to the date of data take. From April to September, L-band copolarized returns vary by as much as 5 dB and the crosspolarized return by about 2.5 dB on the average. The range of variations for C-band is about 3.5 dB for copolarized and about 2 dB for crosspolarized returns. A common feature is that for all channels, the backscattered signal is at its lowest in the September data take. This can be attributed to the low moisture in the canopy and the forest floor at this time of the year.

#### 4.2.1. Trends in estimated values

Figures 7(a)-(f) and 8(a)-(f) show the retrieval results for the real and imaginary parts of the dielectric constant, respectively, for the YJP stand. The stand is outlined in both figures. These are summarized in Figures 9(a) and 9(b), where it is seen that the real and imaginary parts both show an increasing trend (except for the real part in data take 6), although each at a different rate. Note that, from Figures 1 and 2, during the thaw season, especially for the 17 April data, the total radar backscatter is larger than what could be predicted by just considering branch layer volume scattering. This is because the imaginary part of the dielectric constant of the layer is low, hence signals can more easily penetrate through the canopy to the forest floor, which was at the time thawing and very wet, and scattered back from the floor. In this case, although volume scattering constitutes most of the backscattered signal, there are significant contributions from other scattering mechanisms as well. Hence the value of dielectric constant is overestimated to reflect a larger contribution from volume scattering. More work needs to be done in such cases to include the effects of other scattering mechanisms in the estimation algorithm.

Figures 9(a) and 9(b) show the increasing trend in the real and imaginary parts of the dielectric constant from April to August, followed by a small decrease

in September (real part only). The variations in the real part show a more uniform and less pronounced increase than the imaginary part. The “error bars” in this case show the range of variation in the retrieved values within the YJP stand; they are not meant to represent the statistical error associated with the retrieval of the mean value of the dielectric constant. The generally increasing behavior of the branch-layer dielectric constant agrees with the expectation that due to increasing temperatures and thawing, the moisture content of the canopy increases. Air temperature measurements for the months (or parts thereof) of April, May, June, July, and September are plotted in Figure 10. These data were provided by BOREAS AFM-7 group. In particular, Figure 10(a) shows the increasing temperatures in April, which caused the thawing process. This led to an increase in the water content. As a result, the dielectric constant also increased. This effect is stronger in the real part; the imaginary part also increased, but the change is not as clearly indicated in the scale of Figure 9(b). Moving from the thaw to the summer growing season, the real part of the dielectric constant keeps increasing at a similar rate, with the imaginary part now showing an order of magnitude increase relative to the thaw. The reason for this difference in variations of the real and imaginary parts of the dielectric could be related to different temperature dependences of the two [22]. It could also be related to the ion concentrations (in the sapwood region), which has been observed previously to cause different behaviors in the real and imaginary parts of the dielectric [21,25-27]. This is especially true for the results obtained for the September data (data take 6), where it is seen that the real dielectric decreases, whereas the imaginary part increases significantly. Assuming the ion concentrations are high due to the presence of certain minerals in the sapwood region, the conductivity of the branches increases (resistivity decreases), which manifests itself in a higher imaginary dielectric constant. It is unclear how higher ion concentrations affect the real part, nevertheless, the lower real part could be due to reduced moisture in the branch layer in September (end of summer) as well as decreasing temperatures (Figure 10(e)).

#### 4.2.2. Comparison with ground-truth

Having established that the temporal trend in the estimated values of dielectric constant is as expected, the numerical accuracy of the respective values must be verified. In doing so, we note the following:

(1) No direct dielectric constant measurements are available for any of these data. Measurements are available from August 1993, which will not be used here for direct comparison, but to approximate the depth of penetration of electromagnetic waves in the branches given the dielectric constant of the outer layer (Cambium). Conclusions will be drawn as to what value of dielectric is seen by radar, given that it varies as a function of radial depth into the branch.

(2) Water content measurements are available in 1994, but they are not given for any particular data take date used here. The values given are obtained during the summer time, and they will be assumed to approximately apply to the June and July AIRSAR data sets. These water content data will be used along with existing mixing formulas for homogeneous vegetation to obtain values for the dielectric constant of the canopy's branch layer components. Since the dielectric values thus obtained are effective values for the entire scatterer (e. g., a branch), these values need to be interpreted in terms of the dielectric constant that is actually seen by and retrieved from the radar. The discussion to follow will reveal that this is best represented by the dielectric constant of the outer layer.

##### *Dielectric constant measurements*

It has been shown in a previous work [21] that within tree trunks and branches, the moisture content and composition of the woody tissue are often such that the dielectric constant follows a profile similar to that of Figure 11. This figure is taken from [21], and shows dielectric measurements as a function of radial distance into tree trunks at C-band for a white pine stand in New Hampshire. The outer layer, containing a higher amount of water, possesses higher dielectric values than the inner layers. This is true for both C- and L-bands. This variation is more pronounced for the real part than the imaginary part. Similar behavior is true for

branches. Table 2 shows the measurements available for the BOREASYJP stand under study here from August 1993 (BOREASRSS-15 group). These are dielectric values for C- and L-bands, taken at two locations within the branches: one from the outer layer, immediately under the bark (Cambium), and one near the center of the branch (nonCambium). The real part is considerably larger in the Cambium case, with the imaginary part also larger but to a smaller degree. These observations are consistent with Figure 11. Table 2 also lists the needle dielectric constant values, which are seen to be very similar to the Cambium branch dielectrics.

In radar measurements, the value of dielectric constant affecting the scattering process is determined by the combined effects of the dielectric values of various layers inside the scatterers (branches or trunks). To clarify this point, the values of Table 2 will be used to estimate the penetration depth of radar signals into branches with the given Cambium dielectric constant. It can then be concluded whether or not the nonCambium values affect the backscattered signals at all. If the complex dielectric constant is represented as

$$\epsilon = \epsilon_r + i\epsilon_i, \quad (6)$$

$$\epsilon_i = \sigma/\omega$$

where  $\sigma$  is the conductivity and  $\omega$  is the radian frequency, then it can be shown [28] that the penetration depth of signals is bounded by the two values

$$d_{min} = \sqrt{\frac{2}{\omega\mu\sigma}} \quad (7)$$

$$d'' = \frac{2}{\sigma} \sqrt{\frac{\epsilon_r}{\mu}} \quad (8)$$

for highly conductive and slightly conductive cases, respectively. The permeability is represented by  $\mu$  and is usually that of free space. We note that these expressions are derived for a homogeneous medium. In a forest canopy, a significant part of attenuation is a result of scattering and diffraction. Hence, though the above expressions can give us an estimate of the depth of wave penetration, they should be used cautiously, keeping in mind that the calculated depths will be overestimates.

Table 3 shows  $d_{min}$  and  $d_{max}$  for C- and L-bands using the Cambium dielectric constants shown in Table 2. From Tables 1 and 3, the waves do not penetrate into the branches beyond the outer layer at C-band, and hence, the Cambium measurement can be taken to be the appropriate dielectric constant to use at C-band. At L-band, the penetration depth is larger, and given the size of the branches, some penetration into the inner layers can be expected. This amount can be calculated, but the steps are more involved and not in the scope of this paper. However, even if a conservative linear approximation is made, the Cambium and nonCambium values of dielectric constant can be averaged and used as the value seen and retrievable by the radar. This would be very close to the Cambium dielectric constant at C-band. Therefore, it can be stated that the effective dielectric constant seen by the radar at either L- or C-bands is approximately equal to the outer-layer dielectric at C-band in this case. Also, at L-band the effect of scattering from needles is very small, and hence can be ignored when studying the branch-layer volume scattering [12].

#### *Moisture content measurements*

Table 4 lists the moisture content amounts measured by the BOREASTE-6 group for the YJP stand in the summer of 1994. These are given for the top, middle, and bottom portions of the canopy. Both the foliage and the branch moisture contents are given. The values are percent ages as calculated from  $(1 - \text{dry weight/wet weight}) * 100$  and are given for four different age classes within the same stand (the values of 6% for F-age4 (top) and 22% for F-age3 (middle) were considered to be abnormally low and hence not used here). Because of the dense branch layer for this YJP stand, there is no significant contribution from the bottom layer of the canopy [12]. Therefore, only the top and middle sections are considered. The foliage and branch moisture contents are quite similar, hence the moisture content of the entire branch layer is taken to be the average of these values, or about 41%.

There have been several previous studies regarding the dependence of the vegetation dielectric constant on its moisture content. For example, Table 5 shows dielectric values for several moisture contents as derived from the work of Hallikainen et al. [24]. These values are derived for crop-type vegetation (corn leaves),

but in the absence of similar derived relationships for trees, these provide, in the least, a good estimate for branches. These are also in agreement with the results of [29] derived for leaves. Also, C-band values have been measured by Salas et al. [21] for three species of pines found in Durham, New Hampshire, as shown in Figure 12. Note that the horizontal axis of Figure 12 is moisture content represented as the percentage of dry weight (denote by  $mpd$ ). To convert these values to the moisture content values of Table 5, the expression  $(1 - 1 / (mpd + 1)) * 100$  must be used. Also note that there is a large spread around the regression lines in Figure 12. These values are slightly larger than those in Table 5, as predicted above. Since these are taken from actually measured data from conifer stands, and since to our knowledge, specific measurements or models relating the moisture content of the branch layer components (branches and needles) to the dielectric constant of its components are not available for the YJP forest, these data will be used in our analysis. The measurements in Figure 12 were taken from different locations within the same tree, i.e., dielectric vs. moisture measurements were performed as a function of radial distance. Hence, this graph cannot be used directly to relate the dielectric constants retrieved from radar to the moisture content of branches. As discussed earlier, the value of dielectric inverted from the SAR is approximately that of the outer layer of the branch (or trunk, depending on the scattering mechanism) at C-band. If the regression of Figure 12 is used to obtain a moisture content using this value of dielectric constant, the result would merely be the moisture content of the outer layer. Therefore, the dielectric constants retrieved from SAR measurements would first need to be interpreted in terms of an effective or average value, and then used in Figure 12 to obtain the moisture content for the entire branch.

Using the data of Table 2 and Figure 11, it is seen that the real dielectric constant of the inner layers of branches and trunks is about 30% of that for the outer layer. Figure 11 also shows that this inner portion is about twice as thick as the outer layer, i.e.,  $2/3$  of the radial length. Using these values, an average dielectric constant can be calculated based on the values retrieved from AIRSAR data. Denoting the inverted dielectric constant by  $\epsilon_{max}$ , the average value, for the purpose of relating to moisture content only, can be approximated as

$$Re[\epsilon_{ave}] \approx \frac{1}{3} Re[\epsilon_{max}] + \frac{2}{3} (0.3 Re[\epsilon_{max}]) = 0.53 Re[\epsilon_{max}]. \quad (7)$$

For the imaginary part, although a similar conclusion can be made, it will not be as accurate as for the real part from Figure 11. Also, note again that the value of the imaginary part of dielectric is not only dependent on the water content, but also on the mobile ion concentrations within the woody tissue. Hence, it may not be a unique indicator of moisture content. This can also be seen by comparing Figures 11 and 12(b) for the same imaginary parts of dielectric constant. Here, only the real part of the dielectric constant is used to infer moisture content of branch layer components.

Figure 13(a) shows the results of applying Equation (7) to the inverted values of Figure 9(a). The percent moisture content corresponding to these dielectric values is shown in Figure 13(b). These are taken from Figure 12(a) (after proper conversion of horizontal axis), and are average values for three different species of conifers. If these results are compared to the only moisture content measurement available from the BOREAS 1994 campaign, it is seen that for the 11 June data take, where the effective single-branch dielectric was found to be  $18.5 \pm 3.2$ , the moisture content would be  $51\% \pm 6\%$ . The measured value was 41%, which is a very good agreement with the inversion results, considering the errors involved in ground-truth measurements, SAR calibration, and the series of approximations made here. If the same comparison is made with the values of Table 5 at C-band, the corresponding moisture content would be close to 5870, which is still a good agreement.

#### 4.2.3. Temperature dependence of dielectric constant

Experimental observation of vegetation has shown that temperature variations, and in particular, temperature variations between freeze-thaw states, strongly affect the dielectric constant of vegetation [25]. These variations follow a hysteresis loop, i.e., depending on whether the temperature is increasing or decreasing, a different (but similar) path is followed. Here, we are interested in the transition from frozen to thawed states. Measurements have shown that for frozen vegetation, the imaginary part of the dielectric constant is nearly zero, with the real part being very small, yet larger than that of air depending on the material that houses the frozen moisture of vegetation (e.g., woody tissue). As the temperature increases,

no change occurs until the point where the moisture thaws. During this time, both the real and imaginary parts demonstrate a rapid increase. For the imaginary part, this transition occurs at a slightly higher temperature, but is faster, than the real part. The thawed value of dielectric constant is a function of the moisture content in the vegetation and the measurement frequency.

The above behavior is similar to our results from April-September radar data inversions (Figures 9 and 13). During the April thaw season, the average daily temperatures were near zero degrees Celsius. This is the point where the rapid transition in dielectric constant takes place. The few-degree variations from this temperature will be dependent upon the water content and type of vegetation. During this period, the real part of the dielectric constant was making the transition from completely frozen values to the nearly thawed ones. That is why the increasing trend during the three April data takes is observed. In particular, notice the large range in the retrieved values of the real dielectric for the 17 April results as shown by the "error bar." This is due to the fact that in various locations in the canopy, the vegetation might be at slightly different temperatures, and the large variation is a manifestation of the rapid freeze-to-thaw change in the dielectric constant. As for the imaginary part, as mentioned above, the transition takes place at a slightly higher temperature, but in a more rapid fashion. In April, our results suggest that this transition had not yet taken place for the imaginary part, but the June and July results obviously show the thawed values.

As shown in [25], as the temperatures decrease towards freezing (the other branch of the hysteresis cycle), the imaginary part actually increases up to the point where freezing takes place. This could explain the increase in imaginary part of the dielectric constant for our results from September, when the air temperatures in fact decreased (Figure 10). The decrease in the real part during this time could be due to reduced moisture levels, in addition to decreasing temperatures (opposite to the imaginary part).

Besides the above-referenced work, we are not aware of other dielectric vs. temperature measurements more relevant to the YJP scene of BOREAS. The above

cannot validate the accuracy of our numerical estimates, but certainly establishes the integrity of the trends observed. Since the numerical accuracy of at least one of the inverted values was also determined in the previous subsection, all the inverted dielectric values must therefore have good accuracy.

## 5. CONCLUDING REMARKS

An inversion algorithm based on a nonlinear least-squares criterion was used to invert a subset of forest parameters from a parametric model. This model was derived from a discrete component forest scattering model which included all the major scattering contributions. The parametric model only included one of these mechanisms, namely, volume scattering from the branch layer. The free parameters were the real and imaginary part of the dielectric constant of branch layer components. The algorithm was first tested and validated with synthetic data and later applied to six data sets from the BOREAS YJP site. The results clearly indicate the distinct moisture states of the forest canopy at the dates of the data takes. The estimated dielectric constant values were related to moisture content of the branch-layer constituents. These values were in good agreement with the ground-truth measurements performed during the summer of 1994 BOREAS field campaigns. The temperature dependence of dielectric constant was discussed and the corresponding trend in the inversion results was explained,

Several previous studies were used in this paper to relate the inversion results to ground-truth measurements. These were adequate as tools for initial validation of this algorithm, but more comprehensive and specific ground-truth information regarding moisture content and dielectric constant of forest stands, especially as functions of time and temperature, will be needed for more rigorous validations.

This inversion algorithm will later be extended to cases where a larger set of forest parameters will be treated as unknowns, using the same methodology as described here. In its current form, this is a valuable tool for monitoring the change in canopy moisture states for various forest stands over short- or long-term temporal scales.

## ACKNOWLEDGEMENT

The work described here was performed by the Jet Propulsion Laboratory, California Institute of Technology, under a contract from the National Aeronautics and Space Administration. The authors wish to thank S. Durden for providing them with the forest scattering program and A. Freeman for providing the three-component classification algorithm.

## APPENDIX

To solve the nonlinear estimation problem, a number of iterative techniques can be used. Among these are the steepest descent algorithm (gradient method), conjugate gradient method, Davidon-Fletcher-Powell method, and many other Newton-type algorithms. To improve the convergence and robustness characteristics, these algorithms could be "preconditioned." For example, here we have implemented a preconditioned version of the conjugate gradient method, in which the conjugate directions are premultiplied by a conditioning operator. The resulting algorithm is summarized below for the  $n$ -th iteration, with the variable designations used throughout this paper:

$$\begin{aligned}
 \text{(i)} \quad & \mathbf{d}_n = \mathbf{f}_{nl}(\mathbf{X}) \\
 \text{(ii)} \quad & \mathbf{g}_n = \bar{\mathbf{F}}_n^t \cdot \bar{\mathbf{C}}_d^{-1} \cdot (\mathbf{d}_n - \mathbf{d}_0) + \alpha_n \cdot (\mathbf{X}_n - \mathbf{X}_{ap}) \\
 \text{(iii)} \quad & \mathbf{c}_n = \bar{\mathbf{C}}_X \cdot \mathbf{g}_n + \frac{\mathbf{g}_n^t \cdot \bar{\mathbf{C}}_X^t \cdot (\mathbf{g}_n - \mathbf{g}_{n-1})}{\mathbf{g}_n^t \cdot \bar{\mathbf{C}}_X \cdot \mathbf{g}_n} \cdot \mathbf{c}_{n-1} \\
 \text{(iv)} \quad & \alpha_n = \frac{\mathbf{c}_n^t \cdot \mathbf{g}_n}{\mathbf{c}_n^t \cdot \bar{\mathbf{F}}_n^t \cdot \bar{\mathbf{C}}_d^{-1} \cdot \bar{\mathbf{F}}_n \cdot \mathbf{c}_n + \mathbf{c}_n^t \cdot \bar{\mathbf{C}}_X^{-1} \cdot \mathbf{c}_n} \\
 \text{(v)} \quad & \mathbf{X}_n = \mathbf{X}_n - \alpha_n \mathbf{c}_n
 \end{aligned}$$

## REFERENCES

- [1] BOREAS Experiment Plan, Chapter 1, Version 3.0, May 1994.
- [2] A. Freeman, S. L. Durden, and R. Zimmerman, "Mapping Subtropical Vegetation Using Multifrequency, Multipolarization SAR Data," *Proc. IGARSS '92*, Houston, TX, pp. 1986-1689, 1992.
- [3] J. J. van Zyl, "Unsupervised classification of scattering behavior using radar polarimetry data," *IEEE Trans. Geosci. Remote Sensing*, vol. 27, pp. 36-45, 1989.
- [4] S. R. Cloude and E. Pottier, "A review of target decomposition theorems in radar polarimetry," *IEEE Trans. Geosci. Remote Sensing*, in press.
- [5] T. Le Toan, A. Beaudoin, J. Riou, and D. Guyon, "Relating forest biomass to SAR data," *IEEE Trans. Geosci. Remote Sensing*, vol. 30, pp. 403-411, 1992.
- [6] M. C. Dobson et al., "Dependence of radar backscatter on conifer forest biomass," *IEEE Trans. Geosci. Remote Sensing*, vol. 30, pp. 412-415, 1992.
- [7] K. J. Ranson and Q. Sun, "Mapping Biomass of a Northern Forest Using Multi frequency SAR Data," *IEEE Trans. Geosci. Remote Sensing*, vol. 32, pp. 388-396, March 1994.
- [8] M. Moghaddam, S. Durden, and H. Zebker, "Radar Measurement of Forested Areas During OTTER," *Remote Sensing Environ.*, vol. 47, pp. 154-166, Feb. 1994.
- [9] L. Tsang, Z. Chen, S. Oh, R. J. Marks II, and A. T. C. Chang, "Inversion of snow parameters from passive microwave remote sensing measurements by a neural network trained with a multiple scattering model," *IEEE Trans. Geosci. Remote Sensing*, vol. 30, pp. 1015-1024, 1992.
- [10] P. D. Heermann and N. Khazenic, "Classification of multispectral remote sensing data using a back-propagation neural network," *IEEE Trans. Geosci. Remote Sensing*, vol. 30, pp. 81-88, 1992.

- [11] Y. C. Tzeng, K. S. Chen, W. L. Kao, and A. K. Fung, "A dynamic learning neural network for remote sensing applications," *IEEE Trans. Geosci. Remote Sensing*, vol. 32, pp. 1096-1102, 1994.
- [12] M. Moghaddam and S. Saatchi, "Analysis of scattering mechanisms in SAR imagery over boreal forest: Results from BOREAS'93," *IEEE Trans. Geosci. Remote Sensing*, vol. 33, no. 5, pp. 1290-1296, September 1995.
- [13] M. Moghaddam and S. Saatchi, "An Inversion Algorithm Applied to SAR Data to Retrieve Surface Parameters," *Proc. IGARSS '99*, Tokyo, Japan, August 1993.
- [14] M. Moghaddam, "Retrieval of forest canopy parameters for OTTER using an optimization technique," *Proc. SPIE Symposium on Satellite and Remote Sensing*, Rome, Italy, September 1994.
- [15] S. L. Durden, J. J. van Zyl, and H. A. Zebker, "Modeling and Observation of the Radar Polarization Signature of Forested Areas," *IEEE Trans. Geosci. Remote Sensing*, vol. 27, pp. 290-301, 1989.
- [16] S. L. Durden, J. D. Klein, and H. A. Zebker, "Polarimetric radar measurements of a forested area near Mt. Shasta," *IEEE Trans. Geosci. Remote Sensing*, vol. 29, pp. 444-450, 1991.
- [17] R. H. Lang and J. S. Sidhu, "Electromagnetic backscattering from a layer of vegetation: A discrete approach," *IEEE Trans. Geosci. Remote Sensing*, vol. 21, pp. 62-71, 1983.
- [18] Ulaby, F. T., K. Sarabandi, K. McDonald, M. Witt, M. C. Dobson, "Michigan microwave canopy scattering model," *Int. J. Remote Sensing*, vol. 11, pp. 1223-1253, 1990.
- [19] Wang, Y., J. Day, and G. Sun, "Santa Barbara microwave backscattering model for woodlands," *Int. J. Remote Sensing*, vol. 14, no. 8, pp. 1146-1154, 1993.

- [20] Chauhan, N., and R. Lang, "Radar modeling of a boreal forest," *IEEE Trans. Geosci. Remote Sensing*, vol. 29, pp. 627-638, 1991.
- [21] W. A. Salas, K. J. Ranson, B. N. Rock, and K. T. Smith, "Temporal and spatial variations in dielectric constant and water status of dominant forest species from New England," *Remote Sensing Environ.*, vol. 47, pp. 109-119, Feb. 1994.
- [22] F. T. Ulaby and M. A. El-Rayes, "Microwave dielectric spectrum of vegetation - Part II: Dual dispersion model," *IEEE Trans. Geosci. Remote Sensing*, vol. 25, pp. 550-557, 1987.
- [23] A. Tarantola, "The seismic reflection inverse problem," in *Inverse Problems of Acoustic and Elastic Waves*, F. Santosa, Y. H. Pao, W. Symes, and C. Holland, Eds. Philadelphia: SIAM, 1984.
- [24] M. T. Hallikainen, F. T. Ulaby, M. C. Dobson, M. A. El-Rayes, and L. K. Wu, "Microwave dielectric behavior of wet soil - Part I: Empirical models and experimental observations," *IEEE Trans. Geosci. Remote Sensing*, vol. 23, pp. 25-34, 1985.
- [25] M. A. El-Rayes and F. T. Ulaby, "Microwave dielectric spectrum of vegetation, - Part I: Experimental observations," *IEEE Trans. Geosci. Remote Sensing*, vol. GE-25, no. 5, pp. 541-549, 1987.
- [26] R. P. Singh, V. Kumar, and S. K. Srivastav, "Use of microwave remote sensing in salinity estimation," *Int. J. Remote Sensing*, vol. 11, pp. 321-330, 1990.
- [27] L. A. Klein and C. T. Swift, "An improved model for the dielectric constant of sea water at microwave frequencies," *IEEE Trans. Antennas Propagat.*, vol. 25, pp. 1041-111, 1977.
- [28] J. A. Kong, *Electromagnetic Wave Theory*. New York: Wiley-Interscience, 1986.
- [29] C. Mätzler, "Microwave dielectric model of leaves," *IEEE Trans. Geosci. Remote Sensing*, vol. 32, no. 4, pp. 947-949, July 1994.

## Figure Captions

Figure 1. C-band synthetic data generated from the forest scattering model using ground-truth given in Table 1.

Figure 2. L-band synthetic data generated from the forest scattering model using ground-truth given in Table 1.

Figure 3. Error estimates for the retrieval of dielectric constant from the parametric models. (a) Imaginary part assumed known. (b) Real part assumed known. (c) Both real and imaginary parts are allowed to be unknowns.

Figure 4. L-band AIRSAR backscattering data from six different dates in 1994: 1. 17 April, 2. 20 April, 3. 26 April, 4. 11 June, 5. 28 July, 6. 20 September.

Figure 5. C-band AIRSAR backscattering data from six different dates in 1994. 1: 17 April, 2: 20 April, 3: 26 April, 4: 11 June, 5: 28 July, 6: 20 September.

Figure 6. Total power R- G-B overlay of P-L-C bands for the BOREAS jack pine scene in the southern study area. This image was acquired on 28 July 1994. The young jack pine site is shown in white outline.

Figure 7. (a)-(f) Estimated values of the real part of branch-layer component dielectric constant for the six datatake dates. The YJP area is shown in yellow outline.

Figure 8. (a)-(f) Estimated values of the imaginary part of branch-layer component dielectric constant for the six datatake dates. The YJP area is shown in yellow outline.

Figure 9. (a) Real and (b) imaginary parts of estimated dielectric, taken from Figures 7 and 8, for the YJP stand.

Figure 10. (a)-(e) Hourly air temperature measurements near the YJP site for several days before and after each datatake. Data provided by BOREAS AFM-7.

Figure 11. Radial C-band dielectrics and moisture content for a white pine from Durham, NH, 27 September 1991. (Courtesy Salas et al. [20].)

Figure 12. (a) Real and (b) imaginary part of C-band dielectric constant versus , moisture content for low resistance levels (high ion concentration) with regression line ( $r^2 = 0.46$ ). (Courtesy Salas et al. [20]. )

Figure 13. (a) Average, or equivalent, real dielectric and (b) moisture content for the YJP branch-layer components for each of the sic datatakes. Figures 1 1 and 12 were used to obtain these results from Figure 9.

Table 1. Forest parameters from ground-truth measurements

	YJP
tree density (#/m <sup>2</sup> )	1.0
canopy thickness (m)	2.8
trunk height (m)	3.8±0.8
dbh (cm)	4.0±1.4
primary branch density (#/m <sup>3</sup> )	30
primary branch orientation (degrees)	80
primary branch length (m)	0.8±0.22
primary branch diameter (cm)	1.0±0.36
secondary branch density (#/m <sup>3</sup> )	300
secondary branch diameter (cm)	0.4±0.09
needle length (cm)	2.3±0.8
needle diameter (mm)	1.1
needle density (#/m <sup>3</sup> )	5000
soil dielectric constant	(8,1)

Table 2. Dielectric constant measurements in the YJP forest, August '93, RSS15

	Branch, Cambium	Branch, nonCambium	needle
L-band	29.2+i9.0	10.7+i3.9	29.2+i8.7
C-band	19.6+i8.1	5.9+i3.0	20.3+i9.1

Table 3. Penetration depth limits for YJP branches given Cambium dielectric constants given in Table 3.

	$d_{min}(cm)$	$d_{max}(cm)$
<b>L-band</b>	1.8	<b>4.0</b>
<b>C-band</b>	0.4	<b>1.0</b>

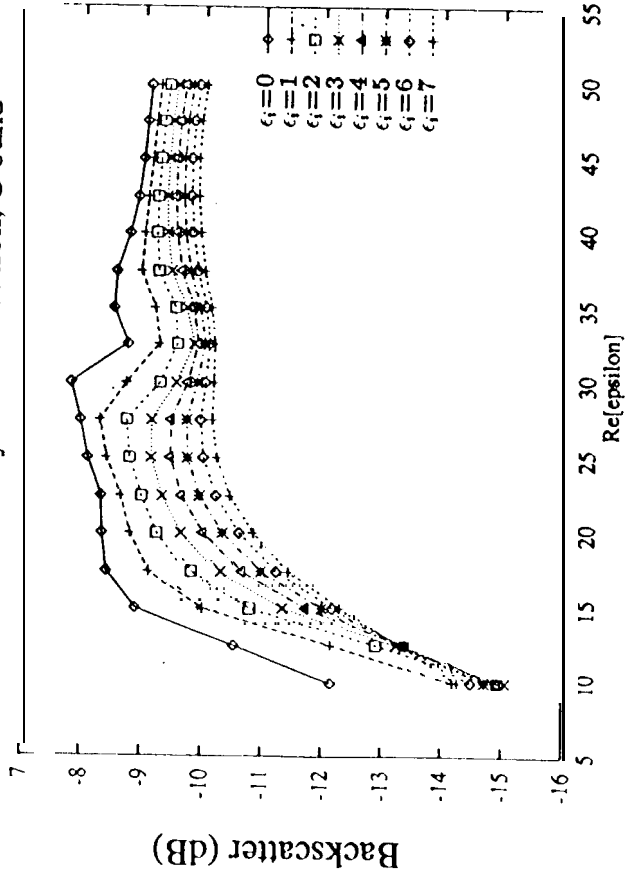
Table 4. Measured moisture content from the top, middle, and bottom sections of the YJP stand, summer '94, TE-??. Values are given in (1-dry weight/fresh weight)\* 100 for foliage (F) and branch (B). The foliage measurements are given for 4 age classes.

	F <sub>age1</sub>	F <sub>age2</sub>	F <sub>age3</sub>	F <sub>age4</sub>	B
<b>Top</b>	38	41	61	6	42
<b>Middle</b>	34	40	22	30	35
<b>Bottom</b>	25	39	42	42	36

Table 5. Complex dielectric constant as a function of vegetation moisture content [23].

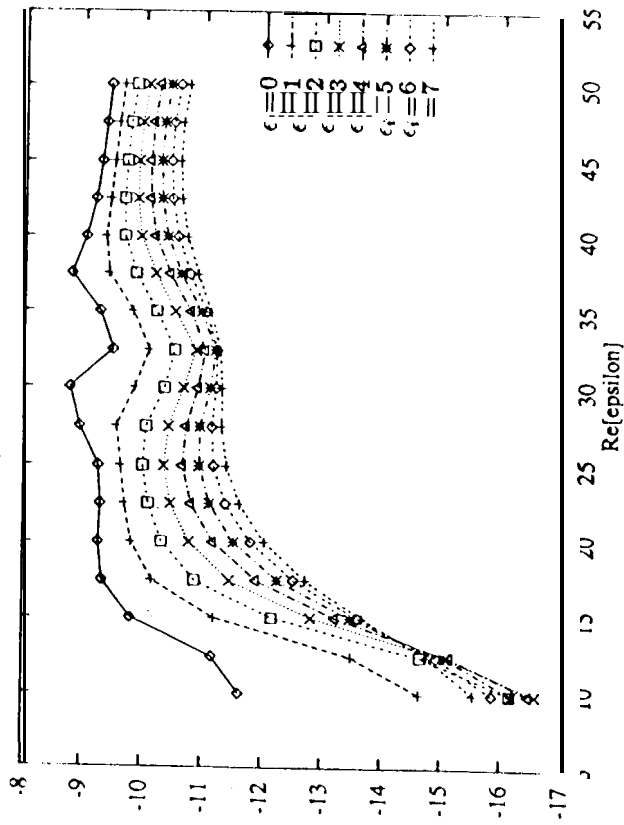
% moisture content	$\epsilon$ , L-band	$\epsilon$ , C-band
22	5.3+i1.7	4.2+i1.2
24	6.0+i2.0	4.7+i1.4
26	6.7+i2.3	5.3+i1.6
28	7.5+i2.5	5.9+i1.8
30	8.3+i2.8	6.5+i2.1
32	9.1+i3.1	7.1+i2.3
34	9.9+i3.4	7.8+i2.5
36	10.8+i3.7	8.5+i2.8
38	11.7+i4.0	9.3+i3.0
40	12.6+i4.4	10.0+i3.3
42	13.5+i4.7	10.8+i3.6
44	14.4+i5.0	11.6+i3.9
46	15.4+i5.3	12.5+i4.1
48	16.4+i5.6	13.4+i4.4
50	17.5+i5.9	14.3+i4.7
52	18.5+i6.3	15.2+i5.0
54	19.6+i6.6	16.2+i5.3
56	20.8+i6.9	17.2+i5.6
58	21.9+i7.3	18.2+i6.0
60	23.1+i7.6	19.3+i6.3

HH Branch Layer Contribution, C band



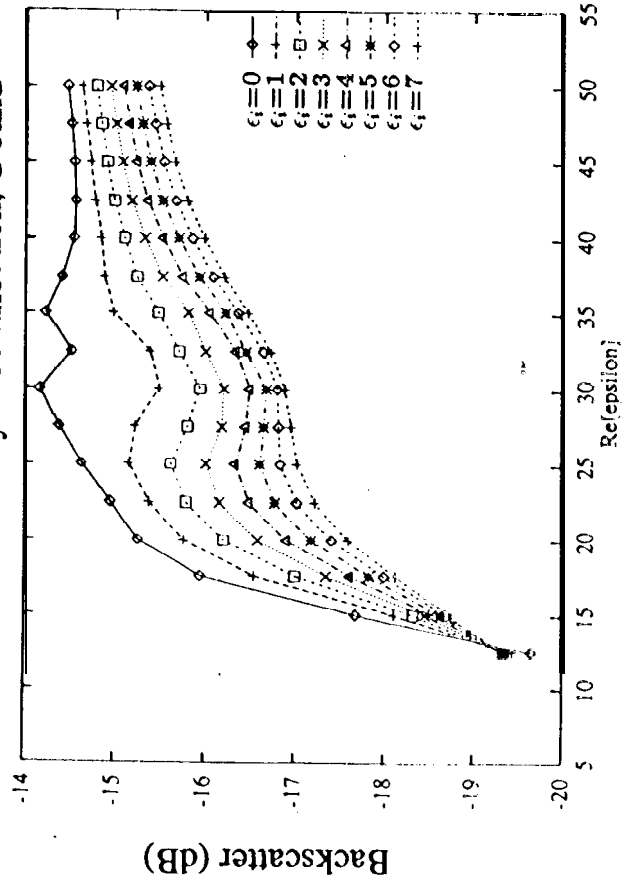
(a)

VV Branch Layer Contribution, C band



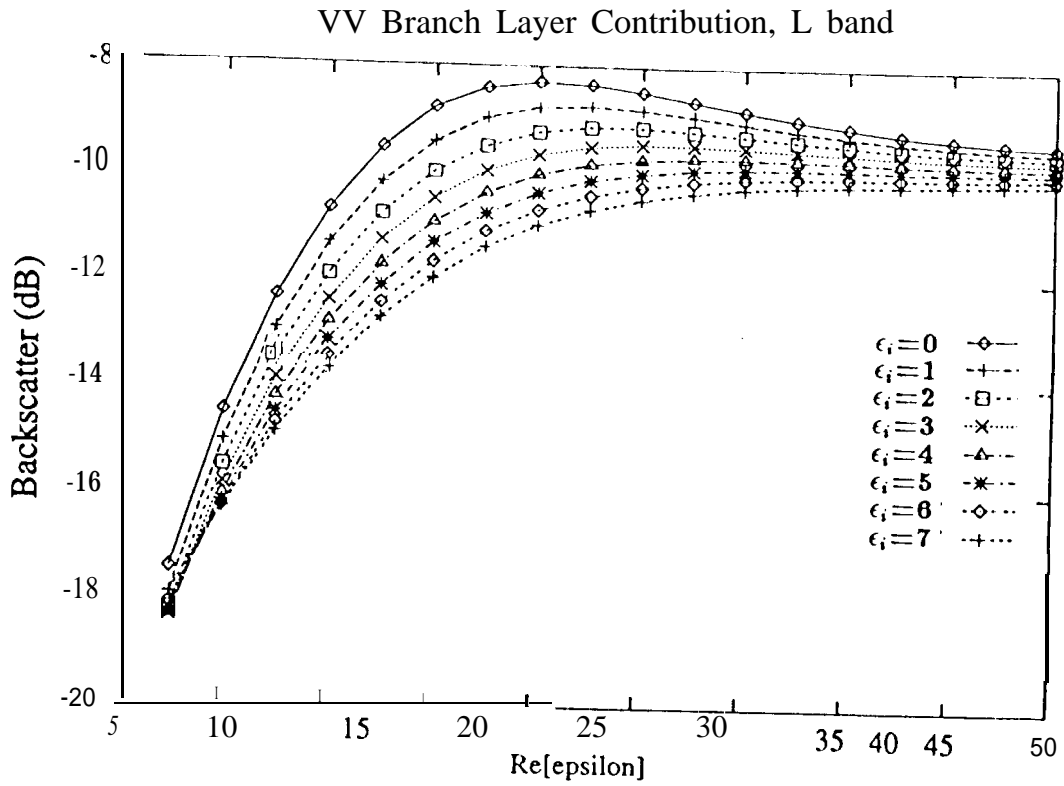
(b)

HV Branch Layer Contribution, C band

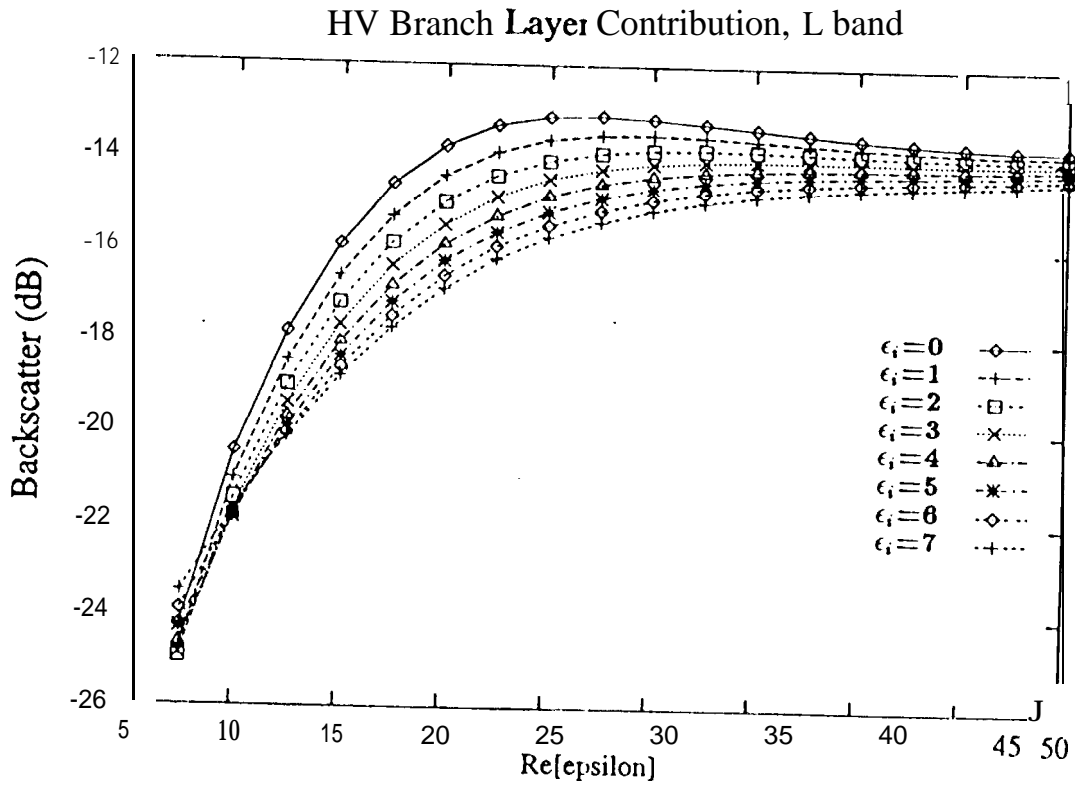


(c)

Fig. 7



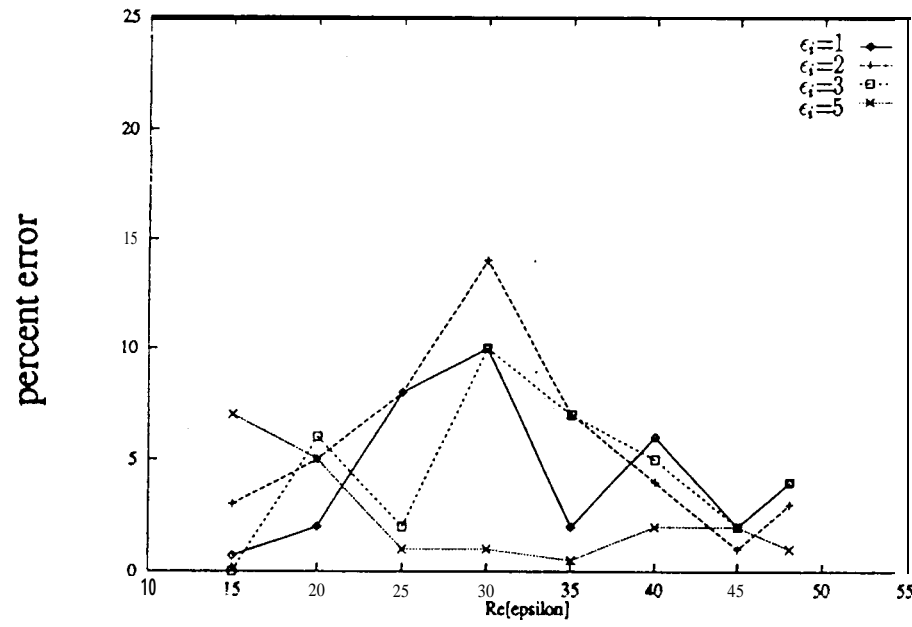
(a)



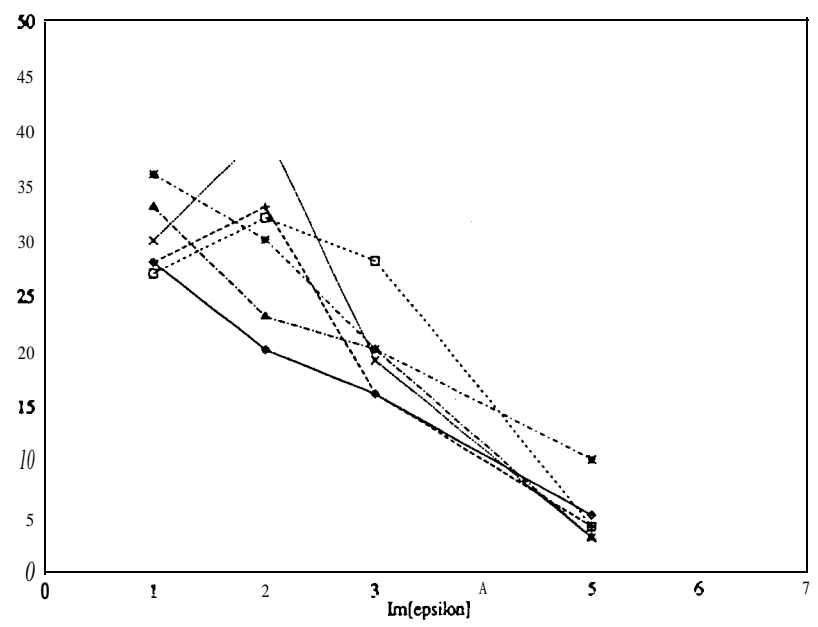
(b)

Figure 2

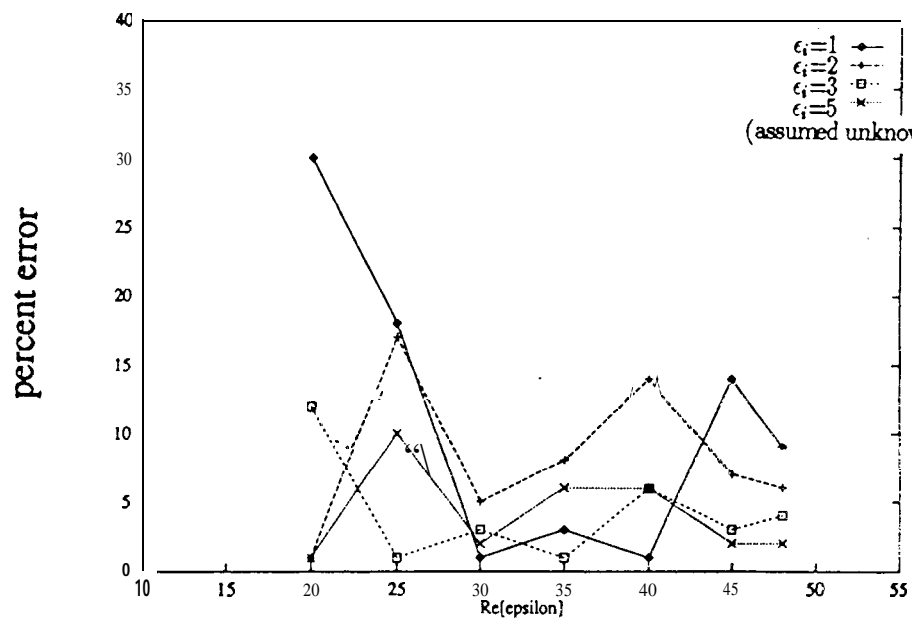
# Accuracy of Retrieval Using Synthetic Data



(a)



(b)



(c)

Figure 3

JPL AIRSAR

SFEN JP 341-1 (J)

TOTAL POWER



SENSOR PARAMETERS

NEAR RANGE, m	8514
A/C ALTITUDE, m	7771
A/C HEADING, deg	-10.9
A/C YAW, deg	-1.2
A/C PITCH, deg	1.0
A/C ROLL, deg	-0.7
BANDWIDTH, MHz	20
PULSE LENGTH, sec	10
FREQUENCY, GHz	PLC
MODE	Quad Pol Mode

DATA PARAMETERS

RUN NAME	South of JP 341 1
DATE ACQUIRED	28 JUL 94
SCENE START GMT	16 10 15
APPROX SCENE CENTER	
LAT	53 DEG 52.9 MIN N
LONG	104 DEG 31.9 MIN W
No RANGE SAMPLES	1279
No AZIMUTH SAMPLES	1024
HDDT INPUT ID	94055
JPL OUTPUT ID	CM4552
PROJECTION	SLANT RANGE

PROCESSING PARAMETERS

PROCESSOR VERSION	3.56
DATE PROCESSED	12 FEB 95
RANGE PIXEL SIZE, m	6.66
AZIMUTH PIXEL SIZE, m	0.24
FRAME COUNT	4121520
PROCESSED YAW, deg	-1.3
PROCESSED PITCH, deg	1.0
PROCESSED ROLL, deg	0.6
PROCESSED ALT, m	7771



1 KM AZIMUTH

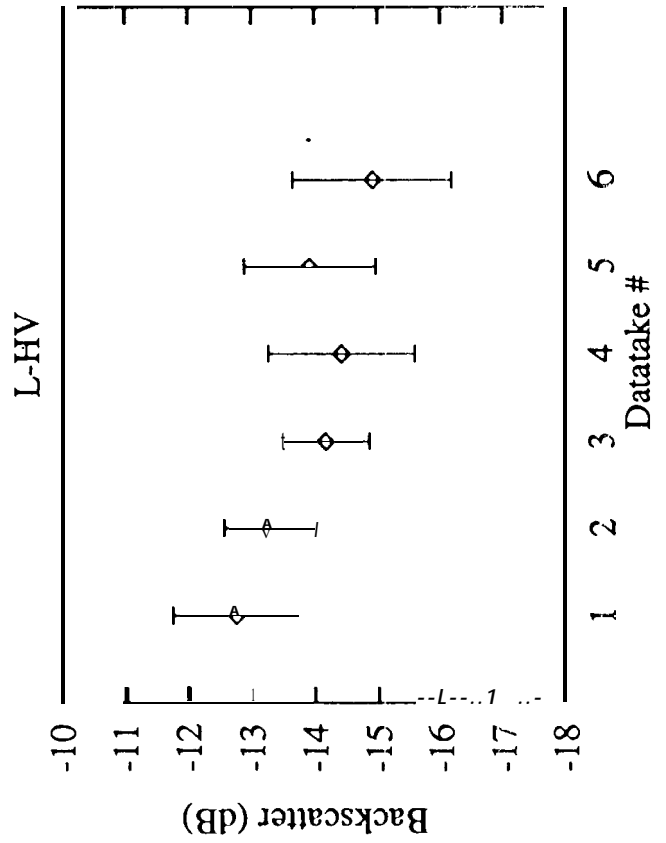
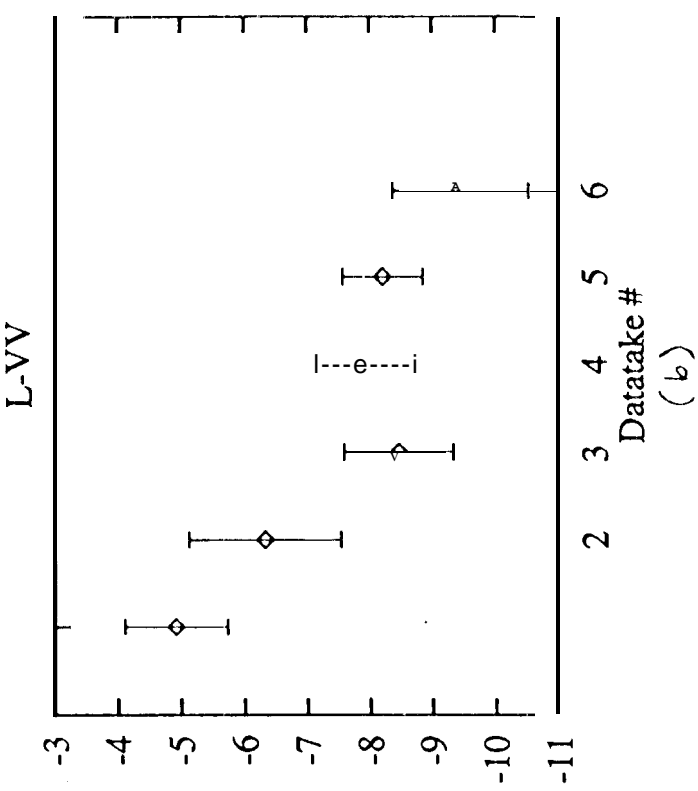
P-BAND (58 cm)

L-BAND (24 cm)

C-BAND (6 cm)

Fig 4

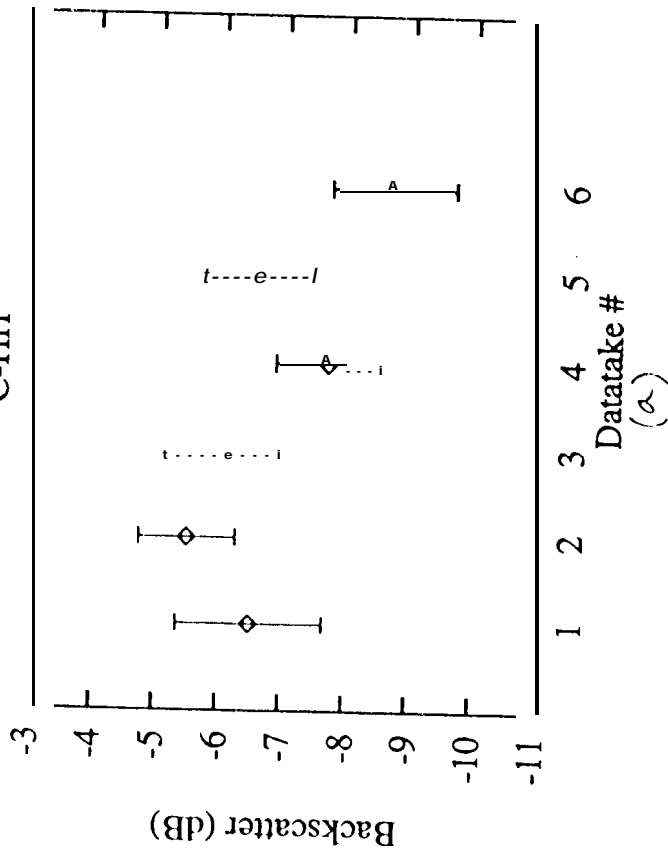
24



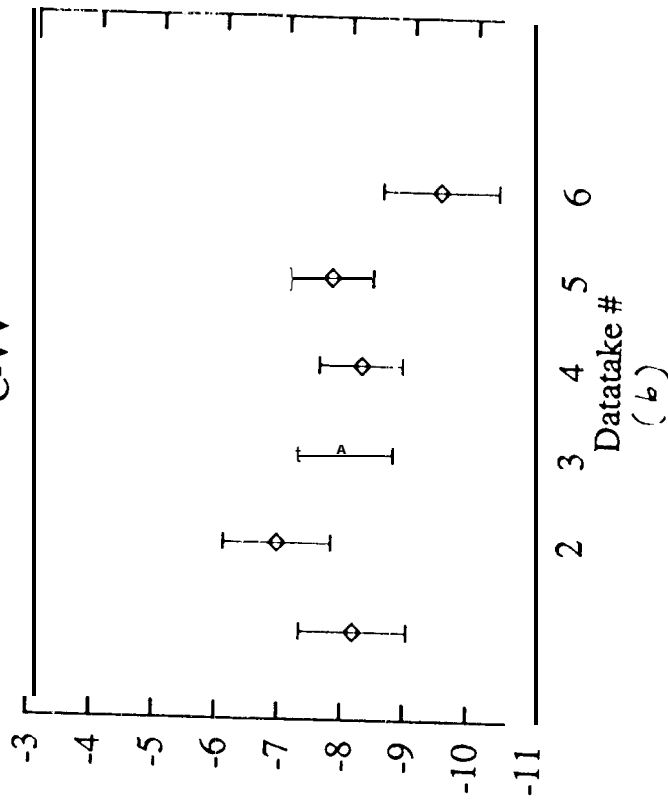
BOREAS SSA YJP AIRSAR Data

Datatake	Date
1	17 Apr 94
2	20 Apr 94
3	26 Apr 94
4	11 Jun 94
5	28 Jul 94
6	20 Sep 94

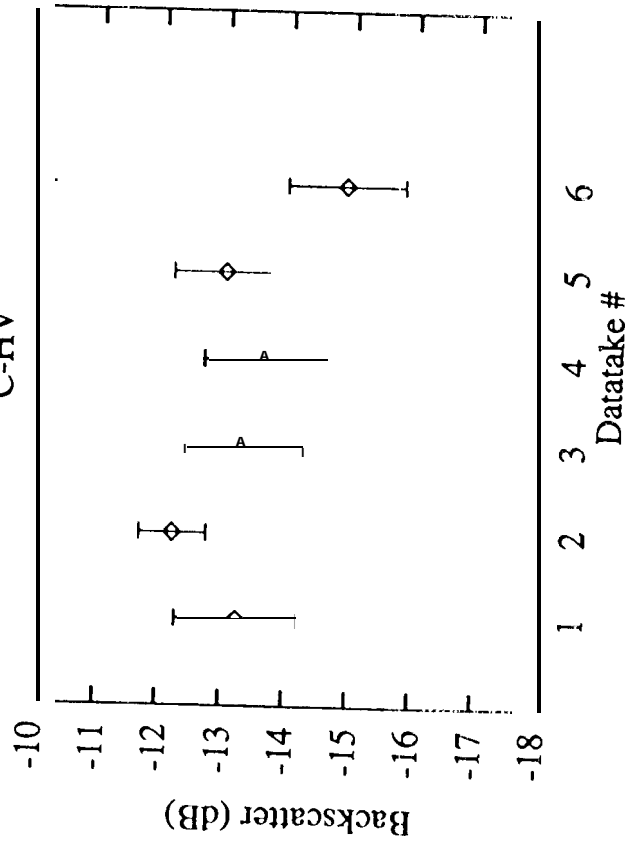
C-HH



C-VV



C-HV



BOREAS SSA YJP AIRSAR Data

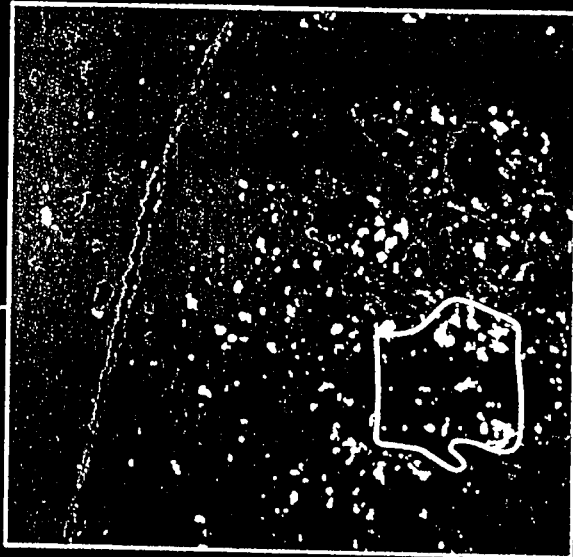
Datatake	Date
1	17 Apr 94
2	20 Apr 94
3	26 Apr 94
4	11 Jun 94
5	28 Jul 94
6	20 Sep 94

Real Part of Dielectric Constant

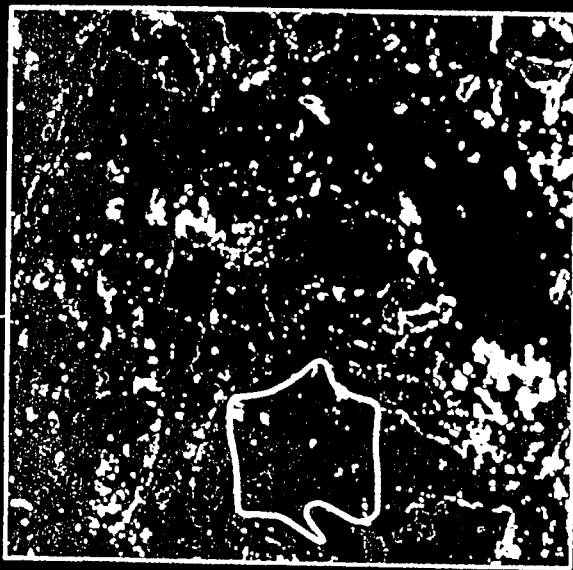
17 April 1994



20 April 1994



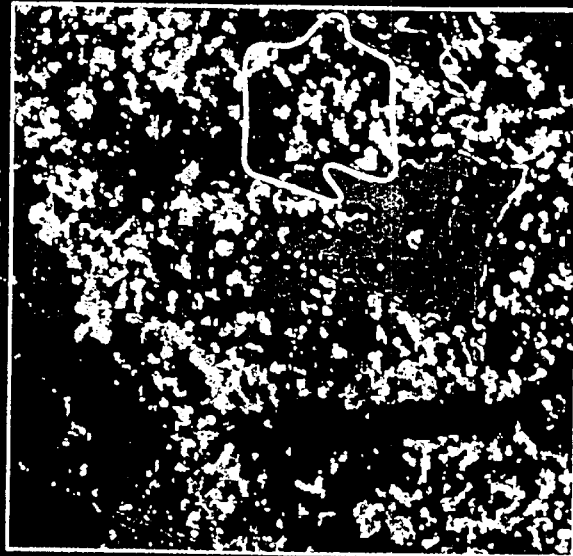
26 April 1994



11 June 1994



29 July 1994



20 September 1994

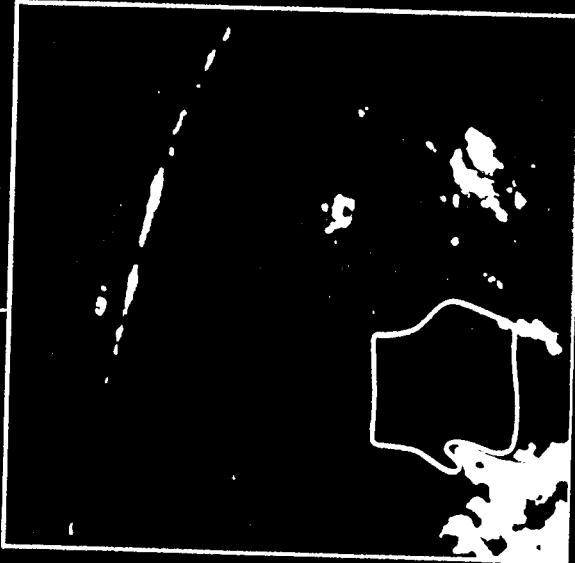


Imaginary Part of Dielectric Constant

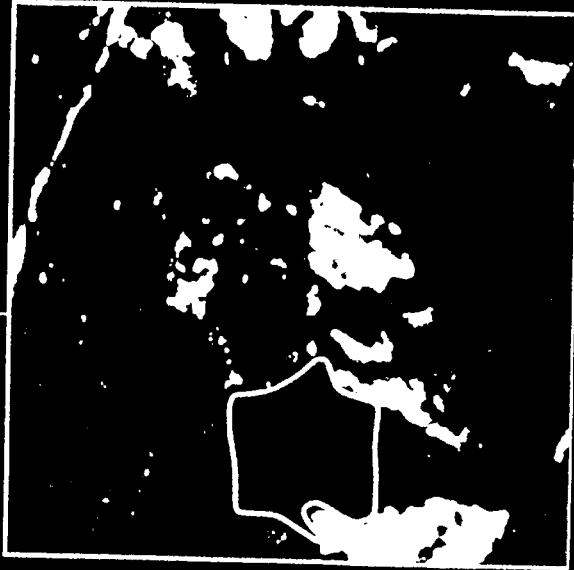
17 April 1994



20 April 1994



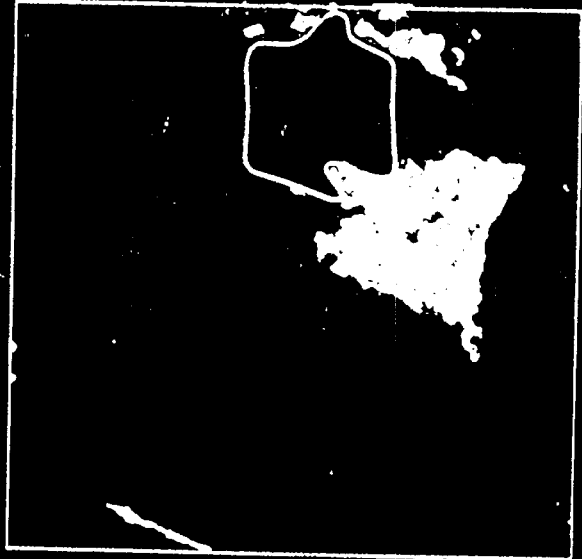
26 April 1994



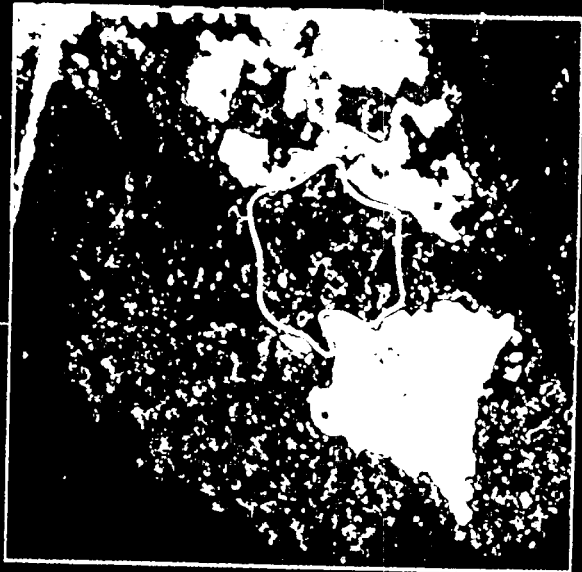
11 June 1994



15 July 1994

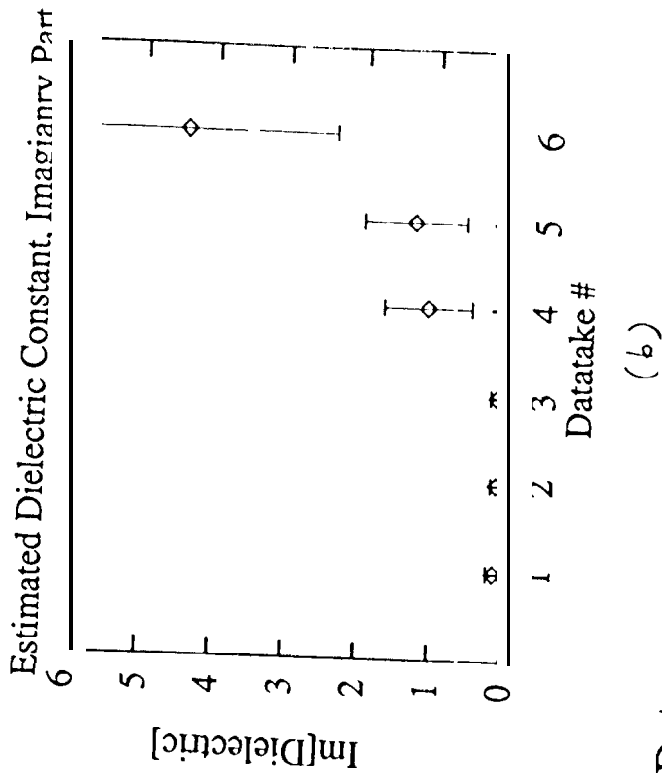
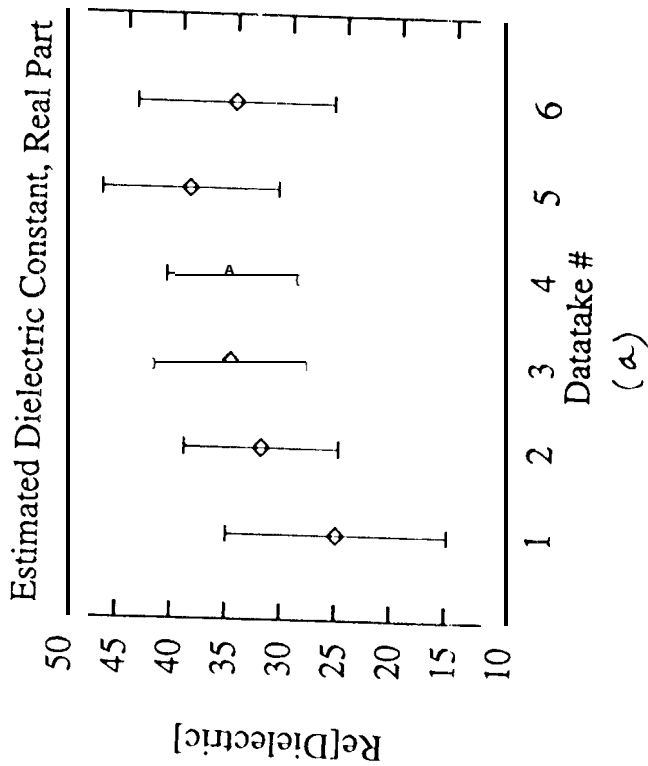


29 September 1994



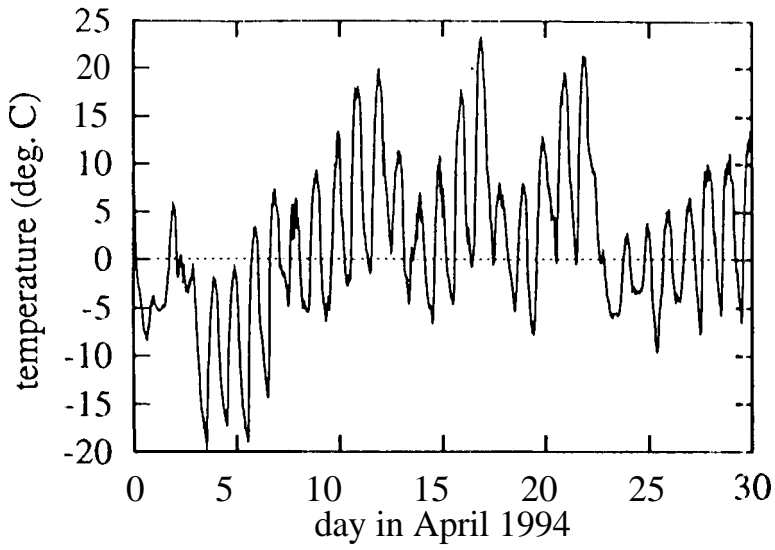
M. MOGHADDAM - JPL

Figure 8

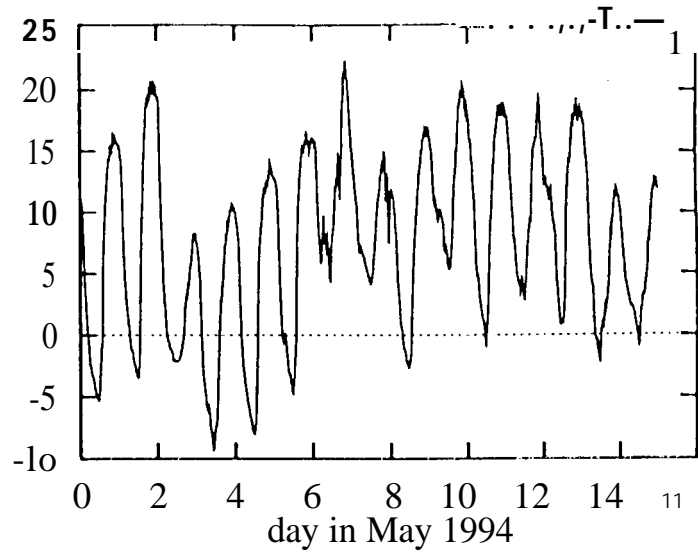


Datatake      Date

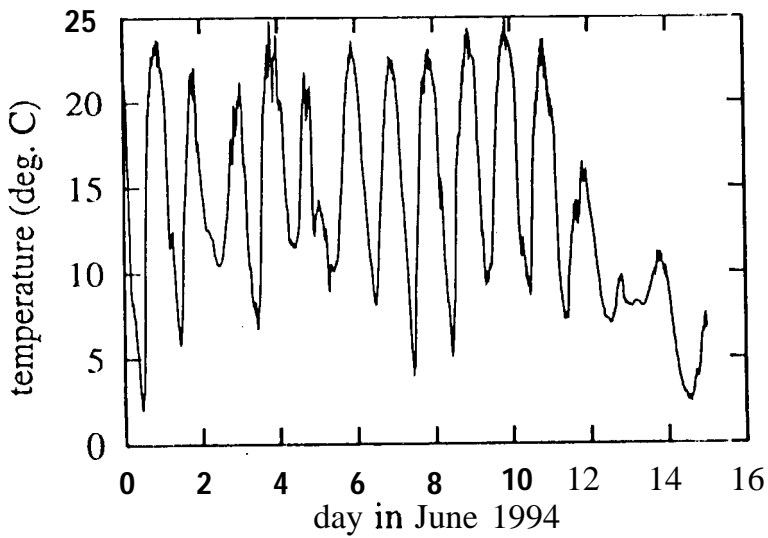
1	17 Apr 94
2	20 Apr 94
3	26 Apr 94
4	11 Jun 94
5	28 Jul 94
6	20 Sep 94



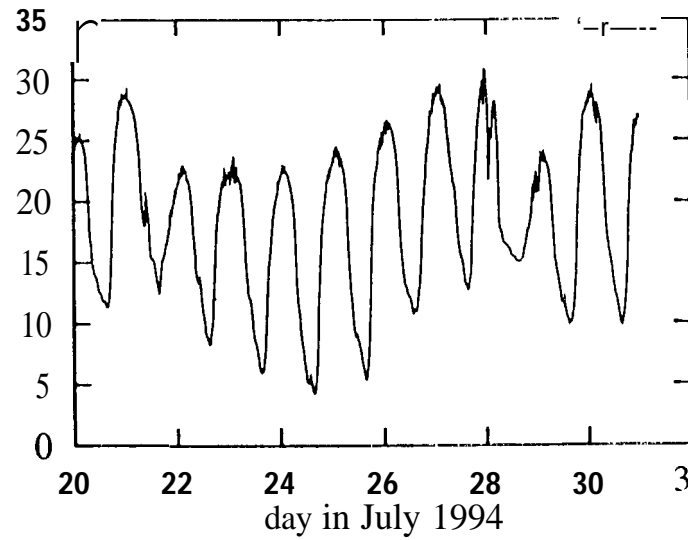
(a)



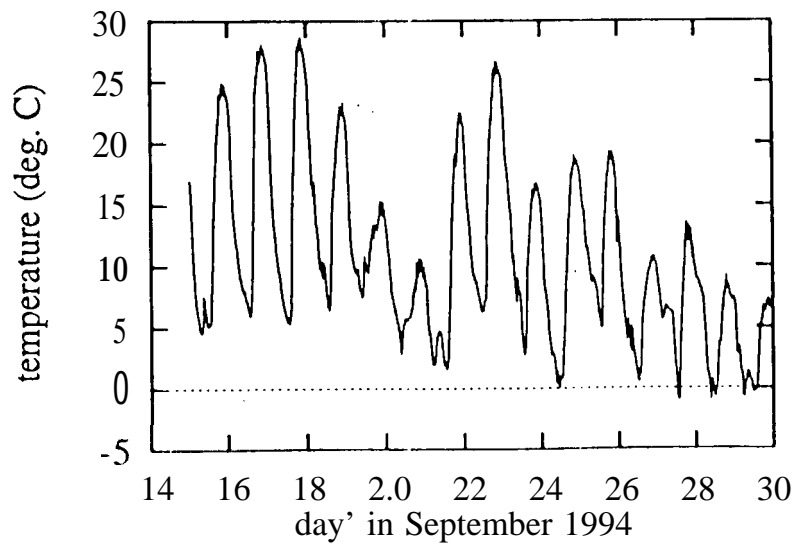
(b)



(c)



(d)



(e)

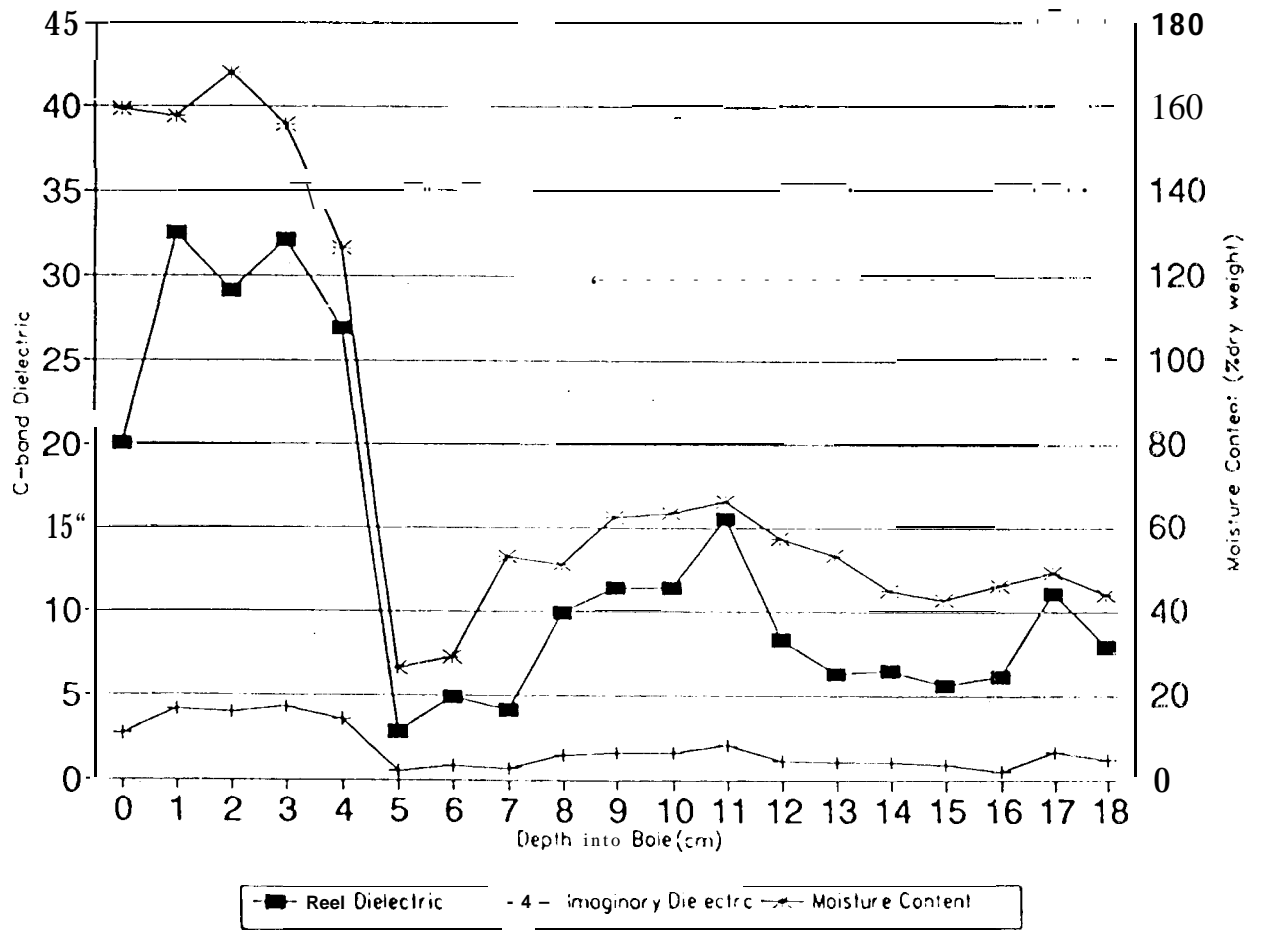
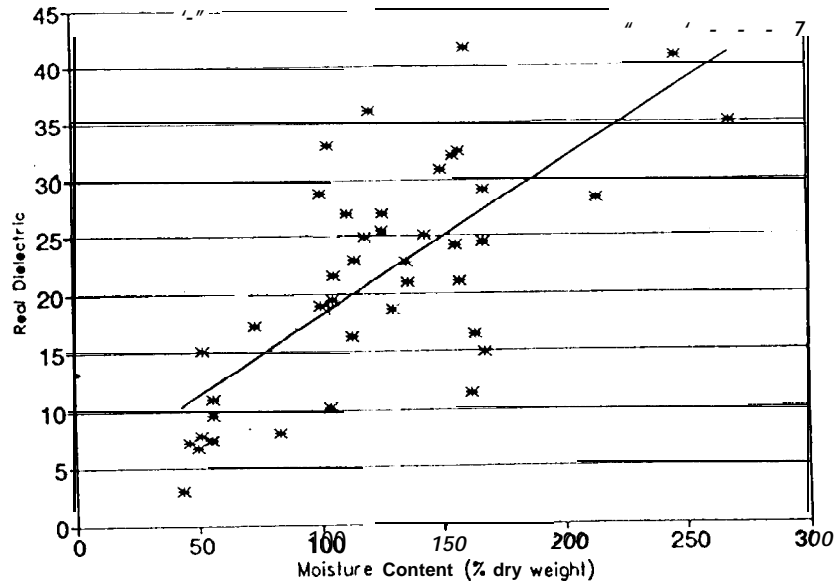
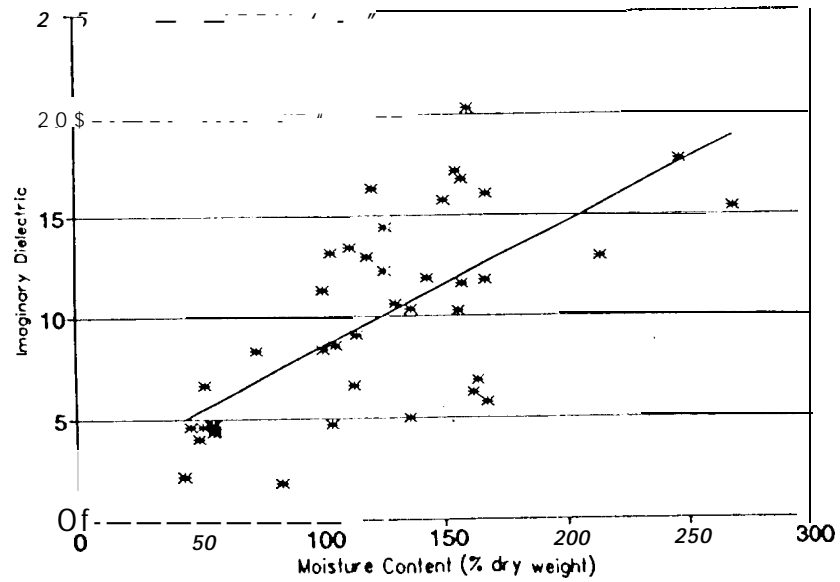


Figure 11

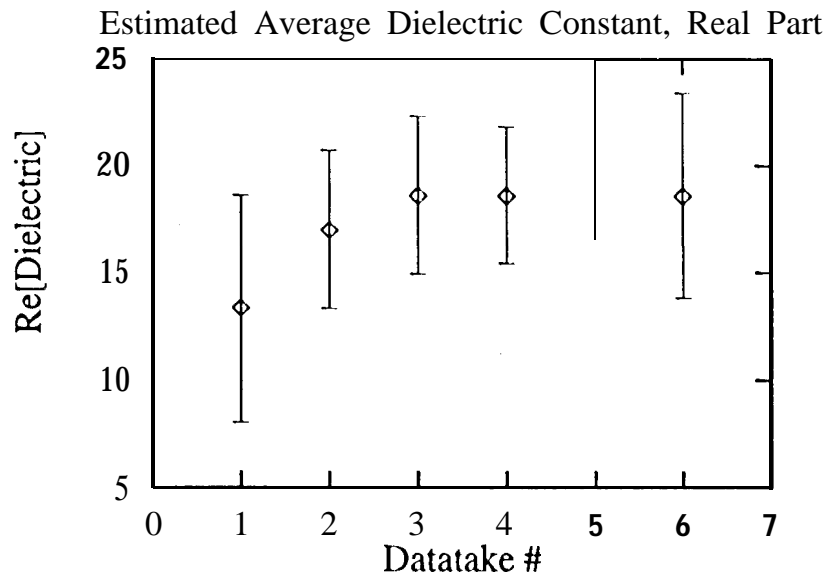


(a)

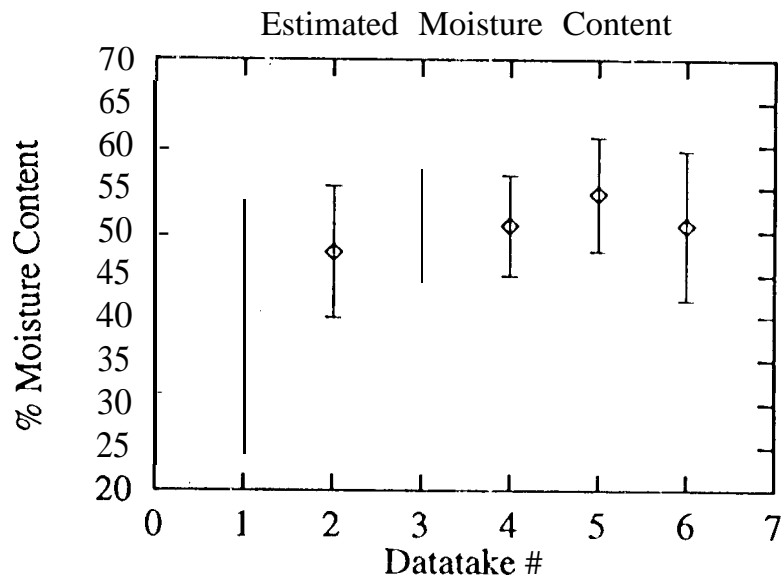


(b)

Figure 12



(a)



(b)

Figure 13